



## RESEARCH ARTICLE OPEN ACCESS

# Voxel-Wise or Region-Wise Nuisance Regression for Functional Connectivity Analyses: Does It Matter?

Tobias Muganga<sup>1,2</sup>  | Leonard Sasse<sup>1,2,3</sup> | Daouia I. Larabi<sup>4</sup> | Nicolás Nieto<sup>1,2,5</sup> | Julian Caspers<sup>6</sup> | Simon B. Eickhoff<sup>1,2</sup> | Kaustubh R. Patil<sup>1,2</sup> 

<sup>1</sup>Institute of Neuroscience and Medicine, Brain and Behaviour (INM-7), Research Center Jülich, Jülich, Germany | <sup>2</sup>Institute of Systems Neuroscience, Medical Faculty, Heinrich Heine University Düsseldorf, Düsseldorf, Germany | <sup>3</sup>Max Planck School of Cognition, Leipzig, Germany | <sup>4</sup>Department of Clinical and Developmental Neuropsychology, University of Groningen, Groningen, the Netherlands | <sup>5</sup>Department of Cardiology, Pulmonology and Vascular Medicine, University Hospital and Medical Faculty, Heinrich Heine University, Düsseldorf, Germany | <sup>6</sup>Department of Diagnostic and Interventional Radiology, Medical Faculty and University Hospital Düsseldorf, Heinrich Heine University Düsseldorf, Düsseldorf, Germany

**Correspondence:** Tobias Muganga ([t.muganga@fz-juelich.de](mailto:t.muganga@fz-juelich.de)) | Kaustubh R. Patil ([k.patil@fz-juelich.de](mailto:k.patil@fz-juelich.de))

**Received:** 25 December 2024 | **Revised:** 25 June 2025 | **Accepted:** 4 August 2025

**Funding:** This work was supported by Helmholtz Portfolio Theme “Supercomputing and Modelling for the Human Brain.”

**Keywords:** connectome-based prediction | denoising | individual differences | individual specificity | preprocessing choices | resting-state functional connectivity | whole-brain parcellation

## ABSTRACT

Removal of nuisance signals (such as motion) from the BOLD time series is an important aspect of preprocessing to obtain meaningful resting-state functional connectivity (rs-FC). The nuisance signals are commonly removed using denoising procedures at the finest resolution, that is the voxel time series. Typically, the voxel-wise time series are then aggregated into pre-defined regions or parcels to obtain an rs-FC matrix as the correlation between pairs of regional time series. Computational efficiency can be improved by denoising the aggregated regional time series instead of the voxel time series. However, a comprehensive comparison of the effects of denoising on these two resolutions is missing. In this study, we systematically investigate the effects of denoising at different time series resolutions (*voxel-level* and *region-level*) in 370 unrelated subjects from the HCP-YA dataset. Alongside the time series resolution, we considered additional factors such as aggregation method (*Mean* and *first eigenvariate* [EV]) and parcellation granularity (100, 400, and 1000 regions). To assess the effect of those choices on the utility of the resulting whole-brain rs-FC, we evaluated the individual specificity (fingerprinting) and the capacity to predict age and three cognitive scores. Our findings show generally equal or better performance for *region-level* denoising with notable differences depending on the aggregation method. Using *Mean* aggregation yielded equal individual specificity and prediction performance for *voxel-level* and *region-level* denoising. When *EV* was employed for aggregation, the individual specificity of *voxel-level* denoising was reduced compared to *region-level* denoising. Increasing parcellation granularity generally improved individual specificity. For the prediction of age and cognitive test scores, only fluid intelligence indicated worse performance for voxel-level denoising in the case of aggregating with the *EV*. Based on these results, we recommend the adoption of *region-level* denoising for brain-behavior investigations when using *Mean* aggregation. This approach offers equal individual specificity and prediction capacity with reduced computational resources for the analysis of rs-FC patterns.

This is an open access article under the terms of the [Creative Commons Attribution-NonCommercial](https://creativecommons.org/licenses/by-nc/4.0/) License, which permits use, distribution and reproduction in any medium, provided the original work is properly cited and is not used for commercial purposes.

© 2025 The Author(s). *Human Brain Mapping* published by Wiley Periodicals LLC.

## 1 | Introduction

In recent years, resting-state functional connectivity (rs-FC) has received increased interest as a representation of individual-level functional brain organization that is predictive of behavior and potentially suitable as a biomarker (Dubois and Adolphs 2016; Finn and Rosenberg 2021). The rs-FC refers to the statistical relationships between spontaneous fluctuations in the blood oxygen level-dependent (BOLD) signal of different brain regions, typically measured with functional magnetic resonance imaging (fMRI), whereas a subject is at rest (Biswal et al. 1995; Friston 2011). For rs-FC to be suitable as an individual-level biomarker, it must be predictive of inter-individual differences and be stable for repeated measurements of the same individual (Finn and Rosenberg 2021; Gordon et al. 2017; Mantwill et al. 2022). Studies have found patterns in rs-FC to be individual-specific (Amico and Goñi 2018; Finn et al. 2015) and stable over extended periods (Gratton et al. 2018; Horien et al. 2019). Additionally, rs-FC patterns have been linked to individual differences in cognitive, behavioral, and clinical attributes (Finn and Constable 2016; Geerligs et al. 2015; Kong et al. 2019; Yamada et al. 2017).

However, capturing meaningful whole-brain rs-FC patterns at the individual level is challenging, as the measured BOLD signal in each voxel is a mixture of neuronal and nonneuronal nuisance signals (Bianciardi et al. 2009; Biswal et al. 2010; Fox and Raichle 2007; Logothetis 2003; Power et al. 2015). Reducing the influence of such nuisance signals is commonly done by removing their variance from the BOLD time series using linear regression (Power et al. 2014). Such removal methods are commonly applied to each voxel's time series, that is the finest resolution, which can be computationally expensive. As rs-FC is calculated using aggregated regional time series, applying the removal process to the regional time series, instead of the voxel time series, offers a potential reduction in computational resources. However, the effect of this choice on the rs-FC and its utility in individual-level analysis has not been explored. Therefore, moving nuisance removal to the regional level requires additional considerations regarding the data quality and the region definition and how it affects the individual specificity and predictability of behavior (Airan et al. 2016; Eickhoff et al. 2018; Finn and Rosenberg 2021; Power et al. 2015; Siegel et al. 2017).

Methods applied on the voxel time series to increase the data quality (i.e., denoising) frequently include removing slow signal drifts, filtering the frequency bands to spectra associated with neuronal signals ( $<0.1$  Hz), and regressing nuisance estimates (Biswal et al. 1995; Leopold et al. 2003; Power et al. 2015). Several nuisance estimates can be derived from different origins; parameters from spatial realignment due to subjects' head motion are often expanded (Friston et al. 1996; Satterthwaite et al. 2013), or signals from non-grey matter are used (Behzadi et al. 2007). Unfortunately, head motion affects voxels nonuniformly across the brain (Power et al. 2017). Therefore, even after using more powerful data-driven estimation of noise components like independent component analyses (ICA; Ciric et al. 2017; Parkes et al. 2018; Salimi-Khorshidi et al. 2014) some motion-related nuisance variance might remain (Bright et al. 2017; Kopal et al. 2020; Power et al. 2015). Performing the removal process at the aggregated regional time series might be advantageous for

stabilizing not only the neuronal signal (Korhonen et al. 2017) but also the motion-related nuisance signal. This stabilized nuisance signal might better match the nuisance estimates, enabling more efficient and effective removal. However, this potential rests on choices of functionally coherent regional representation to enable stable and meaningful interpretability (Airan et al. 2016; Eickhoff et al. 2018; Power et al. 2015).

In order to generate a functionally coherent regional time series, the voxels within a region should exhibit homogeneous functional activity (Stanley et al. 2013). Conversely, functional heterogeneity can arise when multiple nonrelated functional units are captured by the same region definition (Friston et al. 2006; Korhonen et al. 2017). Heterogeneity can arise due to a subject's misalignment to the parcellation or coarse granularities, that is large regions (Craddock et al. 2012). This makes the selection of an aggregation method critical, as its behavior in homogeneous and heterogeneous regions will impact the quality of the rs-FC and in turn the individual differences captured by rs-FC. A common approach to aggregate voxel time series into homogeneous regional time series is averaging all voxel time series in a region, thereby capturing shared aspects by effectively smoothing the time series and reducing complexity (Korhonen et al. 2017). Although straightforward to apply and interpret, it bears the risk of suppressing or canceling relevant variance if the region spans multiple functionally distinct units (Friston et al. 2006). An alternative approach is computing the first eigenvariate (*EV*; Friston et al. 2006). It results from performing eigendecomposition on the voxel time series, resulting in a weighted mean reflecting the main variance component of the regional response (Saxe et al. 2006). In a functionally homogeneous region, the *mean* and *EV* time series are similar (Airan et al. 2016; Saxe et al. 2006). Conversely, in a functionally heterogeneous region, the *EV* will select only the most dominant part of the regional variance (Saxe et al. 2006). The *EV*'s sensitivity can lead to regional time series dominated by a subset of the voxels within the region that might differ from subject to subject (Craddock et al. 2012; Saxe et al. 2006). In the context of individual differences, the *EV*'s sensitivity might be desirable to account for small subject-specific misalignments to region definitions, which are often derived from a group-level atlas. Whether this characteristic is advantageous in the context of the analysis of individual differences is still unclear.

In this regard, the granularity of the parcellation scheme has a considerable impact as the differing sizes of regions affect the functional homogeneity of the regions (Craddock et al. 2012; Shen et al. 2013). With larger regions, more smoothing is applied, which might lead to loss of individual differences (Airan et al. 2016; Finn et al. 2015; Korhonen et al. 2017). On the other hand, a highly granular parcellation might be too close to voxel-level resolution, overemphasizing the impact of residual motion per region, promoting spurious relationships (Power et al. 2015; Stanley et al. 2013) and increasing computational complexity. However, there is no single correct number of regions, as different granularities reflect distinct organizational layers of the brain (Eickhoff et al. 2018), which might impact the stability and predictiveness of individual differences nonuniformly.

To our knowledge, no previous work has investigated the effects of region-wise denoising for individual differences

analyses. Although for *Mean* aggregated regional time series, both voxel-wise and region-wise denoising should result in the same rs-FC patterns at any granularity (Friston et al. 2006), the behavior of *EV* aggregation remains unexplored. To fill this gap, we systematically evaluated the effects of denoising the *voxel-level* and *region-level* time series. We assessed the individual specificity and predictability of individual differences in resulting rs-FC (Finn and Rosenberg 2021). Specifically, we evaluated individual specificity as the ability to identify the same subject from different scans with the binary approach of connectome fingerprinting (Finn et al. 2015) and the continuous approach of differential identifiability (Amico and Goñi 2018). The behavioral predictability was addressed by predictive analysis of age and cognitive test scores acquired outside the scanner. We included considerations to test how known influences such as the quality of the data and parcellation granularity influence *region-level* denoising. To this end, we evaluated the same dataset at two levels of preprocessing affecting data quality and assessed the association of obtained rs-FC with motion, and computed rs-FC with different granularities of the same parcellation scheme. Our comprehensive analyses can inform the design of fMRI processing pipelines and help save computational resources.

## 2 | Methods

### 2.1 | Dataset

The data used for this study was obtained from the Human Connectome Project's Young Adult (HCP-YA) S1200 subject release (Van Essen et al. 2013). The HCP-YA dataset includes two resting-state sessions (R1 and R2) carried out on consecutive days with 30 min of resting-state acquisition per day. Each session involved 2×15-min runs with opposite phase encoding directions (left–right [LR] and right–left [RL]). All subjects' resting-state scans were acquired with a 3T Siemens scanner using the same protocol: slice-accelerated multiband pulse sequence (factor of 8), a spatial resolution of 2 mm isotropic voxels, TR of 720 ms, TE of 33 ms, with a total of 72 slices, a field of view of 208 mm in the anterior–posterior direction, 180 mm in the phase encoding direction (LR and RL), and 144 mm in the inferior–superior direction (for in-depth details on the acquisition protocol, see Glasser et al. 2013; Uğurbil et al. 2013; Van Essen et al. 2013). The HCP-YA scanning protocol was approved by the local Institutional Review Board at Washington University in St. Louis, and all participants provided written consent before participation. Approval for retrospective analysis was given by the ethics committee at the Faculty of Medicine at Heinrich Heine University Düsseldorf (Study No. 2018-317-RetroDeuA). For our investigation, 370 (178 female) nonrelated individuals were selected (by Family\_ID) for whom cognitive scores and rs-fMRI scans from both resting-state sessions (R1 and R2), acquired with both phase encoding directions (LR and RL) were available (Table 1).

#### 2.1.1 | HCP Preprocessing

The HCP-YA resting-state data is accessible ([www.dbconnectome.com](http://www.dbconnectome.com)) at different points throughout the HCP processing

**TABLE 1** | Basic summary statistics for demographics and cognitive variables.

Variable	Statistic
Sex, % ( <i>N</i> )	Male: 52% (192) Female: 48% (178)
Age, <i>M</i> (SD)	28.8 (3.8)
Working memory (ListSort_Unadj), <i>M</i> (SD)	111.8 (11.8)
Fluid intelligence (PMAT24_A_CR), <i>M</i> (SD)	16.9 (4.8)
Reading (ReadEng_Unadj), <i>M</i> (SD)	117.1 (10.8)
Motion (mean FD), <i>M</i> (SD)	0.16 (0.05)

Note: Original variable names specified by the HCP are provided in parentheses.

pipelines. The preprocessing of the HCP-YA dataset has been described extensively elsewhere (Glasser et al. 2013; Smith et al. 2013). In short, the minimal preprocessing pipeline applied by the HCP included the correction of spatial distortion, realignment to correct for head motion to a single-band reference image, distortion field correction, and registration to 2 mm Montreal Neurological Institute (MNI) standard space (MNI152NLIN6Asym). The necessary estimates per step were separately calculated, concatenated, and applied to the fMRI volumes in one spline interpolation to minimize interpolation-induced blurring. The resulting time series were additionally intensity normalized (to a global mean of 10,000) and brain masked (described in detail by Glasser et al. 2013).

The *ICA-FIX* (FMRIB's ICA-based X-noiseifier; Salimi-Khorshidi et al. 2014) denoising pipeline used the minimally preprocessed data as input and removed nonneuronal components from each voxel's time series. This pipeline included temporal high-pass filtering (cutoff at 2000s full-width-half-minimum), FIX classification of 250 independent components (from ICA) into “good” and “bad” components, and regression of “bad” components and 24 regressors derived from motion estimation (Smith et al. 2013).

For our analyses, we used the minimally preprocessed data and the data from the *ICA-FIX*-based denoising pipeline (Smith et al. 2013). This enabled us to do an assessment of the influence of the amount of denoising performed. The two data quality configurations will be respectively referenced as *Minimal* and *ICA-FIX* from here on forward.

### 2.2 | rs-FC Processing

Our rs-FC processing pipelines (Figure 1) considered two main aspects: Denoising and parcellation. After downloading a given subject's volume, voxel-wise time series were extracted with a binarized brain mask generated from the parcellation template using the Nilearn toolbox (Abraham et al. 2014). Next, either denoising or parcellation was performed. As a last step in each pipeline, rs-FC was generated by calculating the Pearson's correlation coefficient between all pairs of z-scored regional time series (Pernet et al. 2013) resulting in a  $N_{\text{Region}} \times N_{\text{Region}}$

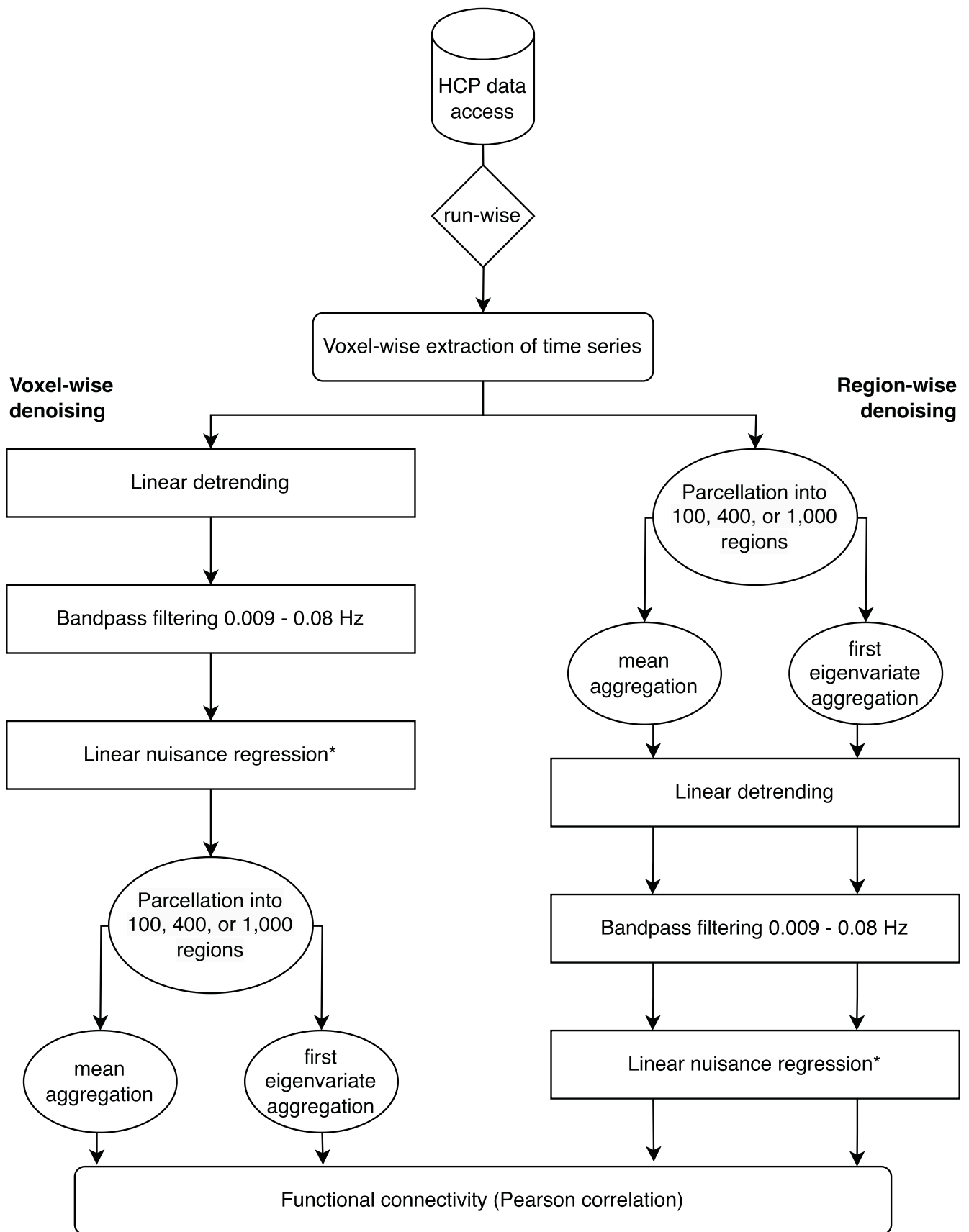


**FIGURE 1** | The schematics illustrate the processing pipelines for voxel-wise and region-wise denoising. Following the download, each phase encoding run is processed independently. Voxel-wise time series extraction precedes either denoising or parcellation. The regressors include WM, CSF, GS, their temporal derivatives, and square terms. \*24 motion regressors were included for the *minimally* preprocessed data configuration only.

correlation matrix. Each subject's rs-FC was computed for each phase encoding run separately.

### 2.2.1 | Voxel-Wise and Region-Wise Denoising

To evaluate differences between denoising the BOLD time series voxel-wise and region-wise, we set up pipelines that differed in two main aspects. Switching the sequence in which these two sections were applied led to the generation of either rs-FC denoised at the voxel level or at the region level. The voxel-wise pipeline (Figure 1, left) denoised all the extracted voxel time series and aggregated the denoised voxel time series into regional time series. The region-wise pipeline (Figure 1, right) aggregated the voxel-wise extracted time series into regional time series first, reducing dimensionality, and applied denoising to the regional time series. In either case, rs-FC was calculated using regional time series that had either been denoised voxel-wise or region-wise.

**2.2.1.1 | Denoising Parameters.** Denoising included the removal of linear trends to correct gradual signal drifts over time, Butterworth bandpass filtering in the frequencies between 0.009 and 0.08 Hz (Kopal et al. 2020; Li et al. 2019; Siegel et al. 2017), and linear nuisance regression. All of these steps were performed using nilearn's "signal.clean" function. A total of 12 nuisance regressors provided by HCP were used consisting of mean signals generated from white matter (WM) and cerebral spinal fluid (CSF) masks as well as the mean global signal (GS; Fox et al. 2009), their temporal derivatives, and their squared terms (Satterthwaite et al. 2013). Although effective at reducing noise, removing GS is heavily debated as it may also remove signals of interest, potentially distorting individual differences (Demertzi et al. 2022; Fox et al. 2009; Li et al. 2019; Macey et al. 2004). However, we decided to include it since removing GS can improve the predictability of behavior from rs-FC (Li et al. 2019; Yan et al. 2013). Additional 24 motion regressors (3 rotations, 3 translations, their 6 temporal derivatives, and 12 squared terms) were included for denoising of the *Minimal* data configuration as HCP's *ICA-FIX*-based denoising pipeline already removed 24 additional motion regressors (Smith et al. 2013). To prevent the reintroduction of artifacts due to the modularity of our setup, nilearn orthogonalizes regressors to the bandpass filter before removal (Lindquist et al. 2019).

### 2.2.2 | Generation of Regional Time Series

**2.2.2.1 | Aggregation Metrics.** Two aggregation metrics were employed to evaluate the ability to capture regional time series, capturing individual differences at different levels of processing. The aggregation into regional time series was either performed on the denoised or the voxel time series. To generate regional time series, all voxel-wise time series from a region were aggregated into one regional time series by computing the *Mean* (Stanley et al. 2013) or the *EV* (Friston et al. 2006). To generate the *EV*, the voxel-wise time series were decomposed using single-value decomposition, and the resulting first eigenvector is sign-adjusted and scaled by the square root of the variance it explains. The variance explained by the first *EV* was

computed by dividing the square of the first singular value by the sum of all the squared singular values.

**2.2.2.2 | Whole Brain Parcellation.** Previous studies suggest that parcellation granularity (i.e., region size) contributes to the ability to identify individual differences (Airan et al. 2016; Finn et al. 2015). Therefore, we generated rs-FC using three different granularities (100, 400, and 1000 regions) of the Schaefer parcellation scheme. The granularities represent the coarsest and finest granularities provided as well as a commonly used intermediary described by Schaefer et al. (2018) to capture fully differentiated regions.

The Schaefer parcellation templates were used ([https://github.com/ThomasYeoLab/CBIG/tree/master/stable\\_projects/brain\\_parcellation/Schaefer2018\\_LocalGlobal](https://github.com/ThomasYeoLab/CBIG/tree/master/stable_projects/brain_parcellation/Schaefer2018_LocalGlobal)) in the Yeo 7-network version in MNI152 (MNI152NLIN6Asym) space (Grabner et al. 2006) to match the data provided by the HCP-YA. This parcellation scheme is based on the resting-state and task-fMRI data of 1489 subjects. Scans between subjects were aligned with surface-based registration, and cortical regions ranging from 100 to 1000 (in steps of 100) were identified with a gradient-weighted Markov Random Field model. The parcellation generated by this approach has been found to produce parcels containing functionally homogeneous voxel time series and with neurobiologically meaningful boundaries, that is they agree well with histologically defined boundaries. The parcellation template was used to mask the voxel-wise extracted time series, assigning labels to each voxel time series. Subsequently, voxel time series with the same label according to the parcellation scheme were aggregated into a regional time series. Subcortical regions were not included in the analysis.

## 2.3 | Stability of Individual Specificity of rs-FC: Identification Accuracy and Differential Identifiability

We assessed the stability of rs-FC in two ways: identification accuracy ( $I_{acc}$ ; Finn et al. 2015) and differential identifiability ( $I_{diff}$ ; Amico and Goñi 2018). First, the rs-FC matrices from the different phase encoding runs were averaged to arrive at one scan per session, resulting in two rs-FC per subject (R1 and R2). Next, we created a  $N_{subject} \times N_{subject}$  identifiability matrix by calculating Spearman correlations between the rs-FC of the two sessions (R1 and R2). In this identifiability matrix, the within-subject correlations are represented by the diagonal values, and the between-subject correlations are represented by off-diagonal values. Identification accuracy was then calculated as the proportion of subjects for whom the highest correlation value was positioned on the diagonal. Differential identifiability was calculated by subtracting the average between-subject correlations from the average within-subject correlations.

To perform statistical comparisons between preprocessing conditions, the raw within-subject ( $n=370$ ) and average between-subject ( $n=370$ ) correlations between R1 and R2 were used. The Fisher z-transformed correlations were evaluated using repeated measures ANOVA. Testing was carried out for each data configuration separately across the factors denoising level, aggregation method, and parcellation granularity. Post hoc group

comparisons were performed as two-sided paired *t*-tests; *p* values were adjusted for multiple comparisons using Bonferroni correction.

## 2.4 | Prediction of Age and Cognitive Scores

To test the effects of denoising the time series voxel-wise or region-wise on brain-behavior predictions, we used the rs-FC obtained from the different preprocessing pipelines to predict age as well as three cognitive measures previously demonstrated to result in reasonable prediction accuracy in the HCP-YA dataset (He et al. 2020; Sasse et al. 2023): *working memory* (ListSort\_Unadj), *fluid intelligence* (PMAT24\_A\_CR), and *reading* (ReadEng\_Unadj). First, each subject's four rs-FC matrices were averaged across phase encoding directions (LR and RL) and sessions (R1 and R2) to generate one rs-FC per subject. The unique edges from this rs-FC matrix (i.e., the lower triangle) were then used as features. A kernel ridge regression model with Pearson kernel was used within a nested 5-fold cross-validation (CV) scheme with 5 repetitions, where the inner 5-fold CV was used to select the l2-regularization parameter. To control for possible confounding influences, we removed variance associated with age, sex, and motion (i.e., framewise displacement [FD]; He et al. 2020) from the cognitive scores in a CV-consistent manner, that is confound regression models were trained on the training data and applied to both training and test data to prevent data leakage (More et al. 2023; Snoek et al. 2019). The prediction accuracy was assessed as Pearson's correlation between the predicted value and the observed value of the target. The prediction pipeline was implemented in Python (Version 3.10.0) using the Julearn package (Version 0.2.6.dev3; Hamdan et al. 2023). Julearn is an extension built on top of scikit-learn (Version 1.1.3; Pedregosa et al. 2011).

To compare the prediction scores statistically, the significance of the group differences was determined using variance-corrected pairwise *t*-tests (Nadeau and Bengio 2003) within each data configuration. The results of these variance-corrected comparisons were additionally corrected using Bonferroni correction to account for multiple comparisons.

## 2.5 | Motion Association Assessment for rs-FC

To understand how the main results might be impacted by residual head motion influences, we also computed rs-FC typicality (TFC; Kopal et al. 2020). TFC evaluates the typicality of an individual rs-FC compared with a group-averaged rs-FC. A higher typicality is associated with lower motion estimates (i.e., mean FD). We used this measure to assess the motion association of rs-FC resulting from our different pipelines. TFC was computed following rs-FC generation for each run separately. TFC values were generated by computing Pearson's correlation of rs-FC to the group rs-FC of the same run. The group rs-FC was generated by averaging all rs-FC from the same run. The association between TFC and FD was assessed by computing the Spearman correlation.

Statistical comparisons were performed on the TFC values. To obtain one value per subject, the scan-wise TFC values

were averaged and Fisher *z*-transformed, followed by a 3-way repeated measures ANOVA per data configuration. Post hoc comparisons were performed using two-sided paired *t*-tests and Bonferroni correction for multiple comparisons.

## 2.6 | Preprocessing Time Assessment

The computation time of each pipeline execution was tracked to compare the runtime. Once the data download was complete, the timer was started before voxel-wise time series extraction and stopped after the generation of rs-FC. To ensure the stability of the measurements per subject, we made sure that all pipelines for a single subject were executed on the same compute node on a high-throughput computing cluster. Although different subjects might have been processed with slightly variable processing power, the speed is stable across all pipeline executions for each subject.

In order to assess differences in runtime for our manipulations, recorded runtimes were averaged across sessions and phase encoding runs per subject ( $n = 370$ ). These values were examined using repeated measures ANOVA. Post hoc comparisons were determined using two-sided paired *t*-tests and Bonferroni correction for multiple comparisons.

## 2.7 | Data and Code Availability

Further details regarding the obtaining of the HCP-YA dataset can be found at: <https://www.humanconnectome.org/>. The preprocessing, analysis, and visualization scripts used in this project are available in the project repository: <https://github.com/juaml/voxel-vs-region-denoising>. The preprocessing pipeline utilized the open-source toolbox Junifer, which is accessible at: <https://github.com/juaml/junifer>. Machine learning-based prediction analyses were conducted using the toolbox Julearn, available at: <https://github.com/juaml/julearn>.

# 3 | Results

## 3.1 | Individual-Specificity of rs-FC Denoised at the Voxel- or Region-Level

Consistent with previous literature using whole-brain rs-FC (Finn et al. 2015; Sasse et al. 2023),  $I_{acc}$  for *voxel-level* denoising ranged from 0.768 to 0.997, whereas *region-level* denoising ranged from 0.945 to 0.997 (Table 2). *Region-level* denoising was equal to or better in identification performance than *voxel-level* denoising in all the cases. For  $I_{diff}$ , the performance for both *voxel-level* denoising and *region-level* denoising ranged from 19.58 to 34.768 (Table 2). For this metric, the *region-level* denoising also obtained better or equal results in all cases except the *EV* aggregation with a parcellation granularity of 100 regions.

The parcellation granularity was an important factor for the identification performance. In all cases,  $I_{acc}$  increased with increasing parcellation granularity.  $I_{acc}$  values were less influenced by parcellation granularity for *Mean* aggregation, ranging from 0.954 to 0.997 for both data quality configurations

**TABLE 2** | Overview of identification performance across all conditions.

Row	Data configuration	Parcellation granularity (regions)	$I_{acc}$ (voxel)	$I_{acc}$ (region)	$I_{diff}$ (voxel)	$I_{diff}$ (region)
<i>Aggregation: EV</i>						
1	<i>Minimal</i>	100	0.802	0.951	22.37	19.67
2	<i>Minimal</i>	400	0.959	0.986	27.954	28.041
3	<i>Minimal</i>	1000	0.982	0.993	31.572	32.552
4	<i>ICA-FIX</i>	100	0.768	0.945	22.286	21.329
5	<i>ICA-FIX</i>	400	0.970	0.987	27.620	30.049
6	<i>ICA-FIX</i>	1000	0.991	0.997	31.722	34.709
<i>Aggregation: Mean</i>						
7	<i>Minimal</i>	100	0.954	0.954	19.587	19.587
8	<i>Minimal</i>	400	0.987	0.987	27.963	27.963
9	<i>Minimal</i>	1000	0.993	0.993	32.530	32.530
10	<i>ICA-FIX</i>	100	0.95	0.95	21.301	21.301
11	<i>ICA-FIX</i>	400	0.987	0.987	30.044	30.044
12	<i>ICA-FIX</i>	1000	0.997	0.997	34.768	34.768

(Table 2). However, for *EV* aggregation, the parcellation granularity had a more pronounced impact in *voxel-level* denoising for both data quality configurations (*Minimal*: 0.802–0.982; *ICA-FIX*: 0.768–0.991). For the parcellation granularity of 400 regions, all identification accuracies were above 0.94, increasing to 0.982 for 1000 regions. The parcellation granularity effect was also prominent in  $I_{diff}$  (Table 2). The performance obtained with the *ICA-FIX* data configuration was better compared with the one obtained from the *Minimal* data configuration, except for the *EV* aggregation in *voxel-level* denoising, where the obtained performance was similar for both data quality configurations.

As expected, the denoising level did not influence  $I_{acc}$  or  $I_{diff}$  for *Mean* aggregation, since the same performance was achieved between the two denoising levels in each parcellation granularity and each data configuration. The performance of the two aggregation methods (*Mean* and *EV*) was found to be almost equal when denoising at the regional level; when the same data configuration and parcellation granularity were used.

Statistical comparisons of the underlying within- and between-subject distributions support the observation of the individual scores. In the within-subject correlations, a three-way interaction of the three factors (denoising level, aggregation method and parcellation granularity) was found separately in both data configurations (for detailed statistical report, see Tables S4 and S5). Post hoc tests showed that within-subject correlations consistently decreased as parcellation granularity increased in both data configurations. Group comparisons between denoising level and aggregation methods showed lower within-subject correlations of the *voxel-level* denoised and *EV* aggregated FCs (for detailed group comparisons, see Table S6). There was also a significant difference between the *region-level* denoised and *EV*

aggregated within-subject correlations in comparison to both *Mean* aggregated groups in the 100 and 400 region parcellation granularity in the *minimally* preprocessed data configuration (Figure S3a,b). In the 1000 region parcellation granularity, these differences were not significant. For the *ICA-FIX* data configuration, this difference was only found in the 100 region parcellation granularity.

In comparison, between-subject correlations showed overall similar trends. The main descriptive difference between within-subject and between-subject correlations was in the magnitude of the differences (for detailed statistical report, see Tables S7 and S8). Results of the repeated-measures ANOVA showed a three-way interaction for between-subject correlations for both data configurations. The general trend of lower values with finer granularities was also present and more pronounced than in within-subject correlations. The same was true for the denoising level and aggregation method, which also showed lower between-subject correlations in *voxel-level* denoising and *EV* aggregation across all parcellation granularities (for detailed group comparisons, see Table S9). The significant differences between the *region-level* denoised and *EV* aggregated between-subject correlations in comparison to both *Mean* aggregated groups were distributed differently (Figure S3c,d). In the *minimally* preprocessed data configuration, the 400 and 1000 region parcellation granularities showed significant differences, whereas in the *ICA-FIX* data configuration, the difference was only significant in the 400 region parcellation granularity.

### 3.2 | Predictiveness of rs-FC Denoised at the Voxel- or Region-Level

In the prediction analysis, age showed the strongest average correlation (0.286) between predicted and actual scores across

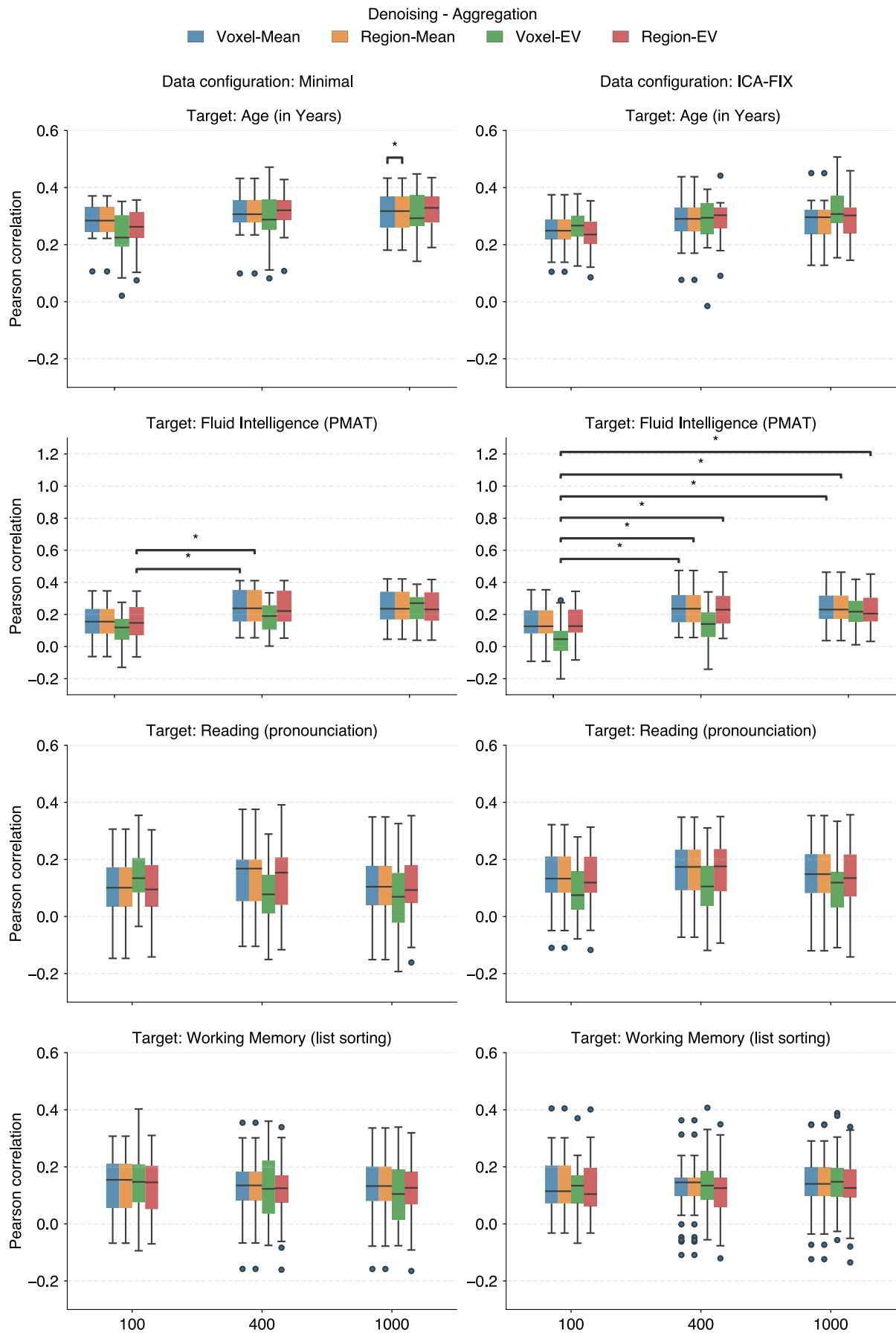


**FIGURE 2** | Legend on next page.

**FIGURE 2** | Prediction scores based on rs-FC denoised voxel-wise or region-wise in both data quality configurations. Scores are calculated as Pearson's  $r$  between the predicted and observed values of each target. Points indicate scores generated over 5-fold  $\times$  5-repeats in each of the three parcellation granularities across two denoising levels and two aggregation methods. Rs-FC was averaged across both runs (LR and RL) and both sessions (R1 and R2) per subject. Variance-corrected pairwise t-test within each data configuration per target revealed significant differences ( $p < 0.05$ ) in the prediction of age and fluid intelligence scores.

all conditions (Figure 2). Among the cognitive scores, *fluid intelligence* had the strongest correlation (0.199), whereas *working memory* and *reading* obtained 0.127 and 0.119, respectively.

Between the two aggregation metrics, small differences in average correlation between predicted and actual scores were also observable for the targets *fluid intelligence* (Mean: 0.215/EV: 0.183) and *reading* (Mean: 0.128/EV: 0.111). As expected, there were no differences between *voxel-level* and *region-level* denoising for *Mean* aggregation (Figure 2). Regarding the *EV* aggregation method, there was no clear difference between *voxel-level* and *region-level* denoising for predicting *age* and *working memory* (Figure 2). However, *region-level* denoising showed a slight advantage for predicting *fluid intelligence* and *reading* (Figure 2).

Similar to the identification analyses, prediction performance increased with increasing parcellation granularity but only for the target *fluid intelligence* (Figure S3). This trend was most noticeable with *EV* aggregation, where *voxel-level* denoising showed increasing performance with increasing parcellation granularity. *Region-level* denoising increased only from 100 to 400 regions, which was also seen in *Mean* aggregation performance.

Testing for statistical differences between model scores revealed significant differences in the scores for *fluid intelligence* in both data configurations and one significant difference in the target *age* for the *Minimal* preprocessed data configuration. For *fluid intelligence* in the *Minimal* preprocessed data configuration, prediction scores from rs-FC generated with *region-level* denoising and *EV* aggregation using 100 regions performed significantly worse compared to the models using rs-FC generated with *Mean* aggregation using 400 regions for *voxel-level* ( $t_{(25)} = -4.09$ ,  $p = 0.0004$ ) and *region-level* ( $t_{(25)} = -4.09$ ,  $p = 0.0004$ ) denoising, respectively. In the *ICA-FIX* data configuration, in contrast, model scores for the model trained using rs-FC with 100 regions and denoised *voxel-wise* with *EV* aggregation performed worse than models trained with rs-FC at finer parcellation granularities (see Table S10). For the target *age*, the model scores from rs-FC generated using *voxel-level* denoising were lower than scores from *region-level* denoised rs-FC ( $t_{(25)} = -4.29$ ,  $p = 0.0002$ ) when using *Mean* aggregation in the 1000 region parcellation granularity.

### 3.3 | Assessment of Motion in rs-FC Denoised at the Voxel- or Region-Level

As motion influences can still be present in preprocessed rs-FC (Siegel et al. 2017; Waller et al. 2017), we analyzed the relationship between the typicality of the rs-FC and mean FD for each run (Table S11). To this end, we sought to determine the

association (Spearman correlation) between TFC and mean FD values (Figure 3). In this context, the difference between the data quality configurations was of particular interest, as they include different degrees of motion correction.

As expected, for *Mean* aggregation, the same association values were obtained for both *voxel-level* and *region-level* denoising ranging between  $-0.112$  to  $-0.206$  (*ICA-FIX*) and  $-0.133$  to  $-0.262$  (*Minimal*). For the *EV* aggregation, rs-FC was also more strongly associated with motion in the *Minimal* data configuration ( $-0.135$  to  $-0.342$ ), compared to the association obtained in the *ICA-FIX* data configuration ( $0.001$  to  $-0.208$ ). Importantly, in all the cases, the motion correlation was lower when using the *ICA-FIX* data configuration ( $0.001$  to  $-0.206$ ) compared to the *Minimal* data configuration ( $-0.133$  to  $-0.342$ ). Interestingly, this difference in data quality configurations was largest in the *voxel-level* denoised rs-FC using *EV* aggregation.

Detailed statistical comparisons of the TFC values supported the observation of the TFC and mean FD relationship. Repeated measures ANOVA revealed a three-way interaction of the three factors (denoising level, aggregation method and parcellation granularity) was found separately in both data configurations (for detailed statistical reporting, see Tables S13 and S14). Post hoc tests showed a decrease in TFC values with increasing parcellation granularity in both data configurations. Group comparisons between denoising level and aggregation methods were dominated by lower TFC values of the *voxel-level* denoised and *EV* aggregated FCs (for detailed group comparisons, see Table S15). There was also a significant decrease in the *region-level* denoised and *EV* aggregated TFC values in comparison to both *Mean* aggregated groups in the 400 and 1000 region parcellation granularity for both data configurations (Figure S12).

### 3.4 | Comparison of Pipeline Runtimes

The comparison of time required to preprocess and calculate the rs-FC matrices showed a three-way interaction ( $F_{(2,738)} = 597.44$ ,  $p = 0.000$ , partial eta squared = 0.6182). Further post hoc testing revealed that using *voxel-level* denoising led to a 1.3-fold runtime increase compared to *region-level* denoising ( $F_{(1,369)} = 5287.24$ ,  $p = 0.000$ , partial eta squared = 0.9348) irrespective of the aggregation method or parcellation granularity (Figure 4). When comparing the two aggregation methods, using *EV* aggregation generally led to a 1.7-fold increase in computation time compared to *Mean* aggregation ( $F_{(1,369)} = 3835.03$ ,  $p = 0.000$ , partial eta squared = 0.9122). An influence of parcellation granularity ( $F_{(2,738)} = 2762.55$ ,  $p = 0.000$ , partial eta squared = 0.8822) was observed exclusively in the context of *EV* aggregation. In this case, the usage of 100 regions demanded 1.7 times the computing time required by 1000 regions (see Tables S16–S18 for detailed statistical reporting).

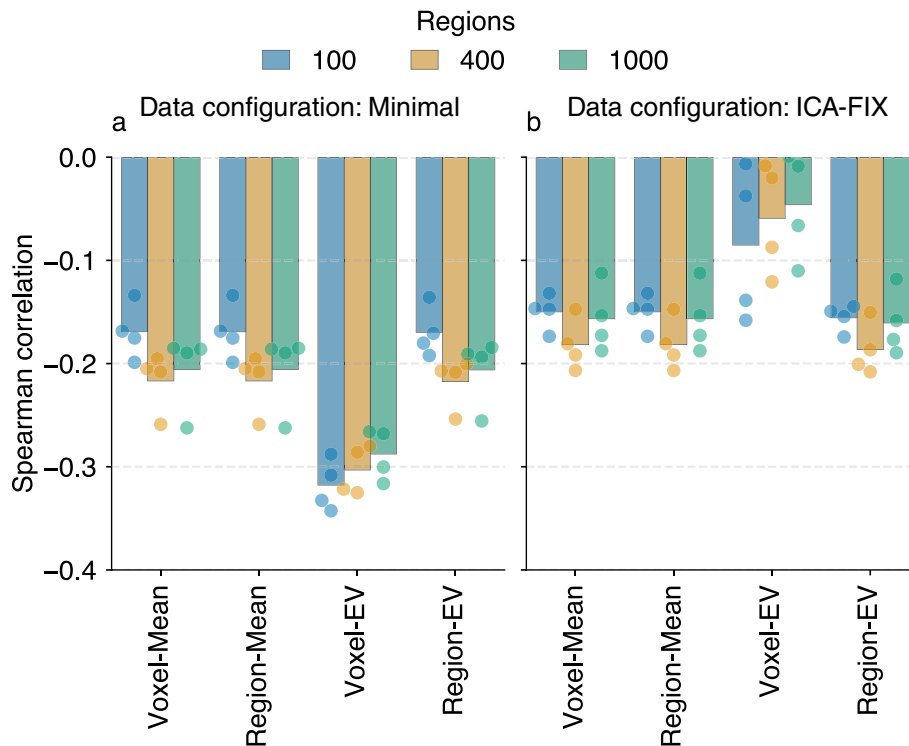


**FIGURE 3** | The association between TFC and mean FD values for all four phase encoding runs in both the *Minimal* data configuration (a) and *ICA-FIX* data configuration (b) is presented across parcellation granularities. Each bar represents the average of all data points. (a) The association was found to be stable for both Mean aggregation and EV aggregation denoised at the region level. However, the association with motion was increased in the EV aggregated rs-FC denoised at the voxel level. (b) The values in the *ICA-FIX* dataset for Mean aggregation and EV aggregation denoised at the region level were stable and exhibited a slight decrease in comparison to those of the *Minimal* data configuration. The EV aggregated rs-FC denoised at the voxel level demonstrated the lowest overall association with motion.

### 3.4.1 | Variance Explained by First Eigenvariate Aggregation

The explained variance for EV aggregation was recorded for descriptive purposes and reporting during preprocessing and is reported in Table S19. The average explained variance per combination of denoising level, aggregation method, and parcellation granularity ranged from 0.458 to 1. A clear separation was observed between voxel-level denoising ( $M=0.5167$ ,  $SD=0.0298$ ,  $Min=0.4579$ ,  $Max=0.5554$ ) and region-level denoising ( $M=0.9999$ ,  $SD<0.0000$ ,  $Min=0.9999$ ,  $Max=1$ ), with the latter consistently showing near-perfect variance explanation. Values in the *minimally* preprocessed data configuration ( $M=0.7514$ ,  $SD=0.2548$ ,  $Min=0.4579$ ,  $Max=1$ ) were slightly lower than those in the *ICA-FIX* data configuration ( $M=0.7653$ ,  $SD=0.2402$ ,  $Min=0.4959$ ,  $Max=1$ ).

## 4 | Discussion

Here, our main goal was to systematically compare denoising on the aggregated region-level versus voxel-level BOLD time series in resting-state processing pipelines for individual-level rs-FC. To take into account other factors influencing rs-FC, we additionally considered two aggregation strategies to obtain regional time series (*Mean* and *EV*), three levels of cortical parcellation granularity (100, 400, and 1000 regions), and two data quality configurations (*Minimal* and *ICA-FIX*). Individual differences in the resulting rs-FC were examined using data from 370

unrelated subjects from the HCP-YA dataset. To assess the utility of the ensuing rs-FC, we evaluated two aspects of individual-level rs-FC: (1) individual specificity quantifying the stability of rs-FC across scans, and (2) the predictability of age, fluid intelligence, working memory, and reading ability. Additionally, we assessed the rs-FC's association with motion as well as computational resources required per pipeline execution. Our results indicated equal or higher performance for region-level denoising with more stable performance and reduced runtime in the *Mean* aggregation strategy. The general performance, especially in individual specificity, increased with increasing parcellation granularity. Not surprisingly, rs-FC from the *Mean* aggregation yields equivalent results for both denoising levels across analyses of individual differences. For rs-FC from EV aggregation, the results between the two denoising levels were dissimilar. This dissimilarity was modulated by the parcellation granularity.

### 4.1 | Individual Specificity of rs-FC Denoised at Voxel- or Regional Level

The usability of whole-brain rs-FC depends on capturing stable individual aspects of brain connectivity which allow reliable identification of the individual across multiple scans (Finn and Rosenberg 2021). Overall the two individual specificity metrics, identification accuracy and differential identifiability, were within the ranges of previous reports (Amico and Goñi 2018; Finn et al. 2015; Sasse et al. 2023). In particular, the high identification accuracy scores (0.95–0.99; see Table 2) are to be

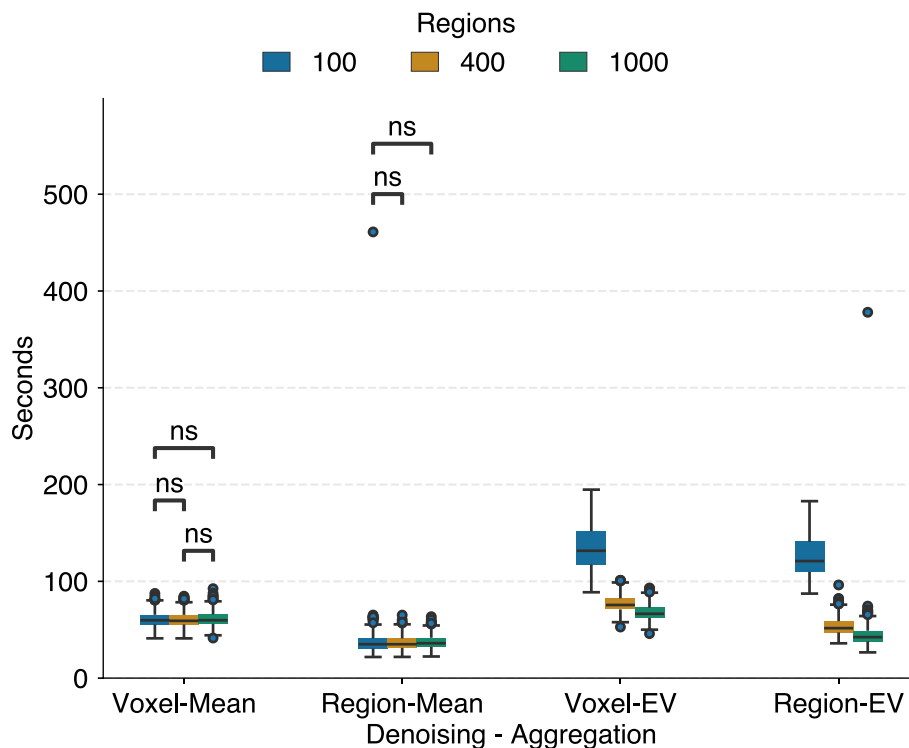


**FIGURE 4** | Pipeline runtime per denoising level and aggregation method across three parcellation granularities. Runtime was averaged across dataset configuration, scan session, and phase-encoding run to generate one runtime per subject ( $n = 370$ ) in each condition. Pairwise  $t$ -tests between all groups were significant ( $p < 0.05$ ) until indicated otherwise. Bonferroni correction was applied to control for multiple comparisons. For Mean aggregation, runtime did not differ between parcellation granularities within denoising levels. Across denoising levels, the runtime was fastest for region-level denoising. For *EV* aggregation, runtime decreased with finer parcellation granularity in both denoising levels. Again, region-level denoising was faster than voxel-wise denoising. Overall, fastest runtimes were achieved with region-wise denoising using Mean aggregation.

expected given the high data quality and long scan duration of the HCP-YA dataset (Airan et al. 2016; Horien et al. 2018). As expected, the performance of *Mean* aggregation for *voxel-level* and *region-level* denoising was equal in all cases. As pointed out by Friston et al. (2006), from the mathematical point of view, this is expected, as long as all steps performed are linear transformations of the data.

The individual specificity improved with finer parcellation granularity. This is in line with previous suggestions that a finer parcellation granularity benefits the identification of individuals in rs-FC (Airan et al. 2016; Finn et al. 2015). Especially, the finer parcellations (400 and 1000 regions) led to almost similar individual specificity across denoising levels and aggregation strategies. As finer granularities contain smaller regions, they are more likely to enclose functionally homogeneous voxels. In cases like this, the behavior of *Mean* and *EV* aggregation has been suggested to be similar (Craddock et al. 2012; Saxe et al. 2006).

However, the coarser parcellation (100 regions) showed a noteworthy difference between *voxel-level* and *region-level* denoising for *EV* aggregation. This difference was characterized by reduced  $I_{acc}$  and increased  $I_{diff}$  in *voxel-level* denoised rs-FC. Although most reports on individual specificity focus on *Mean* aggregated rs-FC, Airan et al. (2016) comparison of *Mean* and *EV* aggregation reported no noteworthy differences between the two aggregation strategies across a similar range of parcellation granularities. Their investigation focused on the amount of data

(acquisition minutes) needed to maximize individual specificity in a sample of 23 subjects. To this end, they compared the two aggregation strategies in a 1000-region Craddock parcellation (Craddock et al. 2012). Their finding of similarity between *Mean* and *EV* is consistent with our findings of individual differences at the finest parcellation granularity (1000 regions). In addition, we have shown that the difference between the two aggregation strategies is greater at coarse parcellation granularity and when using a larger sample size with a similar amount of data per subject. In particular, the sample size has been suggested to affect measures of individual specificity, as a larger number of subjects also increases the likelihood of observing similar rs-FC between subjects (Li et al. 2021; Waller et al. 2017).

Borrowing from the previous arguments of Craddock et al. (2012) and Saxe et al. (2006), the *EV* will select a subset of voxel time series per region in heterogeneous regions, which may lead to the selection of different voxels across multiple scans. This session specificity could lead to an increased likelihood that single individuals get misidentified in a binary test-retest metric such as  $I_{acc}$ , where a single mismatch is enough to influence the overall score. The differential identifiability's ability to quantify the individual specificity on a continuous scale across the whole dataset could still be rather high in this scenario, as long as the mismatch is caused by only one or a few other subjects being more similar.

The suggested behavior of the *EV* only led to individual differences in *voxel-level* denoising. Aggregating the voxel time

series first and then denoising the *region-level* time series led to individual specificity performance similar to *Mean* aggregation. Since denoising involves detrending, effectively demeaning the time series, the *EV* is influenced to select slightly different variance components depending on the denoising level. In the case of *region-level* denoising, aggregating the voxel time series might lead to the *EV* decomposition selecting the regional mean signal, since this component explains the largest amount of variance.

## 4.2 | Predictability From rs-Fc Denoised at Voxel- or Regional Level

Another aspect of rs-FC for effective use in clinical applications is its utility in predicting individual-level demographics and phenotypes (Finn and Rosenberg 2021). In our study, the prediction accuracies (Pearson's *r*) between 0.286 and 0.119 (Figure 2) were in line with previously reported ranges for whole-brain rs-FC-based predictions (He et al. 2020; Sasse et al. 2023). The similarity observed in individual specificity between *voxel-level* and *region-level* denoising when using *Mean* aggregation was also observed for the prediction accuracies across all targets. Thus, the predictive utility of rs-FC did not change irrespective of *voxel-level* or *region-level* denoising. Nevertheless, *voxel-level* denoising is widely used in brain and behavioral studies as common toolboxes (SPM (Friston et al. 2007), FSL (Jenkinson et al. 2012), and CONN (Whitfield-Gabrieli and Nieto-Castanon 2012)) use it as their default. However, due to the mathematical equality, there seems to be no obvious reason to choose one or the other in terms of prediction performance.

The differences observed in the *EV* aggregation were present only in the targets *fluid intelligence* and *reading*. The rs-FC that is optimal for individual specificity is not necessarily optimal for prediction accuracy because different aspects of the signal might contribute to these different goals (Finn and Constable 2016; Noble et al. 2019). Similar or slightly lower prediction accuracies were obtained for *EV-aggregated* rs-FC denoised at the *voxel* level. This suggests that *EV-aggregated* rs-FC does not offer an advantage in prediction analysis. Thus, the potentially interesting ability to capture session-specific details by *EV* aggregation did not uncover patterns that would lead to better predictions of the behavioral targets or age.

Of the four targets, only fluid intelligence was affected by the parcellation granularity. Previous studies have demonstrated that the frontal-parietal network is a driving factor for individual specificity as well as fluid intelligence (Amico and Goñi 2018; Finn et al. 2015). Our results suggest that this alignment between individual specificity and predictability is only meaningful for the prediction of fluid intelligence scores, while other targets might rest on different aspects of the rs-FC. In this target, the lowest parcellation granularity (100 regions) performed worst across the denoising levels and aggregation strategies. The slight improvements with finer granularities suggest that the relevant signal might not be adequately captured at coarse granularities. Interestingly, increasing to finer parcellation did not lead to improved performance at 400 and 1000 regions. Here, it is possible that in large feature spaces, like the 1000-region parcellation, the signal might become diluted; that

is many features might not be associated with the target, and consideration of the curse-of-dimensionality (Hastie et al. 2009) can harm predictive performance (Schulz et al. 2024).

## 4.3 | Additional Considerations

### 4.3.1 | Motion Association

Previous studies suggest that residual motion may influence the individual specificity and predictability of rs-FC (Siegel et al. 2017; Waller et al. 2017). However, others suggest that this influence is likely to be minimized with a sufficient amount of data per subject (Airan et al. 2016; Horien et al. 2018). Our main findings support this view, as we observed stable individual specificity and predictive performance regardless of the degree of preprocessing (*Minimal* or *ICA-FIX*) applied to the raw data by the HCP (Glasser et al. 2013; Smith et al. 2013). In addition to our main findings, we examined the quality of each of the rs-FC runs and its relation to motion by associating the typicality of the rs-FC of each run with the respective average FD (Kopal et al. 2020). Some stable and low degree of association remained in all *Mean* aggregation rs-FCs and the *EV* aggregated rs-FC using *region-level* denoising. These associations have also been reported previously (Kopal et al. 2020). Interestingly, the *voxel-level* denoising in *EV* aggregated rs-FC displayed differing patterns between the two data quality configurations. In the *minimally* preprocessed data configuration, the association to motion was the highest, whereas some of the associations in the *ICA-FIX* data configuration were close to zero. The respective underlying TFC values, however, suggested that these subjects were atypical compared to the group. This could mean that *EV aggregation* is more sensitive to scan-wise influences unrelated to motion, as represented by mean framewise displacement. Further investigation is needed to understand this complex interaction. Since this trend was stable across the parcellation granularities (Figure 3), we take this result as an indicator that, indeed, the *ICA-FIX* data configuration is less motion-associated. However, the decrease in motion did not translate into performance improvement in our prediction analysis (Figure 2).

### 4.3.2 | Pipeline Runtime

In general, the denoising of the regional time series requires less computational time, as shown by the runtime of the different pipelines. The most noticeable difference in runtime was between the aggregation strategies. The *Mean* aggregation strategy had a constant runtime across all levels of parcellation granularity. In contrast, the *EV* aggregation took more time when coarser parcellation granularities (i.e., more voxels per region) were involved. This difference is likely due to the *Mean* strategy being easier to perform, making it efficient regardless of the number of voxels in a region. In contrast, singular value decomposition determines all eigenvectors, of which the first is projected back into the time series domain, which is much more time-consuming. This is especially true when a larger number of voxels are involved in the calculation, as the time complexity of standard *EV* implementations increases with the number of voxels.

#### 4.4 | Limitations and Considerations for Future Work

It should be noted that while we discuss the differences between voxel-wise and region-wise denoising, the *ICA-FIX* pipeline by the HCP was applied to the voxel time series. Hence, our results only account for the additional denoising steps of detrending, bandpass filtering, and linear nuisance regression. Future studies are needed to demonstrate that the obtained results are generalizable to other datasets with differing data quality and scan durations, which are known to influence individual difference analyses (Airan et al. 2016; Horien et al. 2018). Since *Mean* aggregation should be the same for *voxel-level* and *region-level* denoising based on firm mathematical reasons and supported by our empirical demonstration, it should lead to similar outcomes in other datasets. However, the performance of the *EV* might vary depending on multiple factors such as motion content and choice of region size. The influence of these factors was already observable in the current dataset. First indicators of this can be derived from the small shifts in variance explained by the first *EV*. Note that while *ICA-FIX* leads to clean data and is a HCP-specific configuration, the results from the *minimally* processed data configuration might be considered more similar to standard-quality clinical datasets. For future examination, it might be interesting to further investigate the behavior of the *EV* and the potential use of multiple *EVs* to capture higher variance per region.

Here we employed parcellation schemes with three levels of parcellation granularity and found that the largest improvement in identification performance happened between 100 and 400 regions. It might be of interest for future investigations to probe the space between these two granularities. Lastly, as a group-level parcellation was used, it is possible that voxel-to-region assignment across subjects was suboptimal, which might have influenced the *EV* aggregation more than the *Mean* aggregation. Individual-specific region definition approaches might provide better region specification (Kong et al. 2021). Furthermore, additional steps can be performed in rs-FC processing (e.g., scrubbing) that we did not consider. Future work might consider those aspects more closely.

It should be noted that our study focuses on whole-brain FC analyses. The application in other types of analyses (e.g., voxel-to-region analysis) is not considered. However, we are confident that the statements in the context of *Mean* aggregation also apply. It should be noted that it is at the discretion of the investigator whether different pipelines for preprocessing individual seed voxels and target regions are appropriate.

In all our analyses, the fully weighted whole-brain FC matrices per subject were reduced to the upper triangle and then vectorised in order to investigate influences of preprocessing decisions on individual specificity and predictive performance. Future work might extend this investigation into analyses such as thresholded networks that have been shown to perform better than predicting from the connectivity of the whole-brain (Finn et al. 2015; Thiele et al. 2024). Another interesting approach not considered is the use of topological information instead of functional connectivity (Yoshimoto et al. 2024) for prediction analysis. Future studies could address this aspect and investigate

effects in the context of influences and potential benefits of the topological characteristics of brain connectivity.

In this study, our primary focus was not on optimizing individual model performance, but rather on how our manipulations might translate into changes in predictive performance. To this end, we did not emphasize testing of the individual models' predictive capabilities, which could likely be enhanced with further tuning and optimization. This decision was in part also motivated by practical considerations around computational efficiency. To explore a wide range of conditions, we aimed for a streamlined experimental setup that could offer meaningful insights without incurring excessive resource demands. Future work might build on our presented findings and incorporate strategies to enhance individual model performance.

## 5 | Conclusion

Based on our findings, we encourage the potential of denoising time series at the regional level for the analysis of individual differences. Particularly for *Mean* aggregation, as it provides equivalent results and is computationally more efficient. This offers substantial benefits in computational runtime without compromising the individual specificity and predictability of *Mean* aggregated rs-FC. Although *EV* aggregation might be an interesting alternative, the sensitivity to residual motion should be closely monitored and evaluated, especially with voxel-wise denoising. Lastly, the choice of parcellation granularity (i.e., region size) should be carefully considered specifically for *EV* aggregation, as individual differences may suffer in coarser parcellations. With this work, we hope to provide evidence to guide researchers in choosing the most appropriate and efficient steps for investigating brain-behavior associations in future investigations.

### Author Contributions

**Tobias Muganga:** conceptualization, data curation, formal analysis, investigation, methodology, project administration, software, validation, visualization, writing – original draft preparation, writing – review and editing. **Leonard Sasse:** data curation, formal analysis, methodology, software, validation, visualization, writing – review and editing. **Daouia I. Larabi:** conceptualization, supervision, writing – original draft preparation, writing – review and editing. **Nicolás Nieto:** visualization, writing – review and editing. **Julian Caspers:** supervision, writing – review and editing. **Simon B. Eickhoff:** conceptualization, funding acquisition, supervision, writing – review and editing. **Kaustubh R. Patil:** conceptualization, funding acquisition, investigation, methodology, supervision, validation, writing – original draft preparation, writing – review and editing.

### Acknowledgments

This work was partly supported by the Helmholtz Portfolio Theme “Supercomputing and Modelling for the Human Brain.” Data were provided [in part] by the Human Connectome Project, WU-Minn Consortium (Principal Investigators: David Van Essen and Kamil Ugurbil; 1U54MH091657) funded by the 16 NIH Institutes and Centers that support the NIH Blueprint for Neuroscience Research; and by the McDonnell Center for Systems Neuroscience at Washington University. Open Access funding enabled and organized by Projekt DEAL.

## Conflicts of Interest

EiC is co-author—Simon B. Eickhoff is the Editor-in-Chief of HBM and co-author on this article. Simon B. Eickhoff was excluded from the peer-review process and all editorial decisions related to the publication of this article.

## Data Availability Statement

The data that support the findings of this study are available from the human connectome project. Restrictions apply to the availability of these data, which were used under license for this study. Data are available from <https://db.humanconnectome.org/> with the permission of the human connectome project.

## References

- Abraham, A., F. Pedregosa, M. Eickenberg, et al. 2014. "Machine Learning for Neuroimaging With Scikit-Learn." *Frontiers in Neuroinformatics* 8: 14. <https://doi.org/10.3389/fninf.2014.00014>.
- Airan, R. D., J. T. Vogelstein, J. J. Pillai, B. Caffo, J. J. Pekar, and H. I. Sair. 2016. "Factors Affecting Characterization and Localization of Interindividual Differences in Functional Connectivity Using MRI." *Human Brain Mapping* 37, no. 5: 1986–1997. <https://doi.org/10.1002/hbm.23150>.
- Amico, E., and J. Goñi. 2018. "The Quest for Identifiability in Human Functional Connectomes." *Scientific Reports* 8, no. 1: 1–14. <https://doi.org/10.1038/s41598-018-25089-1>.
- Behzadi, Y., K. Restom, J. Liao, and T. T. Liu. 2007. "A Component Based Noise Correction Method (CompCor) for BOLD and Perfusion Based fMRI." *NeuroImage* 37, no. 1: 90–101. <https://doi.org/10.1016/j.neuroimage.2007.04.042>.
- Bianciardi, M., M. Fukunaga, P. van Gelderen, et al. 2009. "Sources of fMRI Signal Fluctuations in the Human Brain at Rest: A 7T Study." *Magnetic Resonance Imaging* 27, no. 8: 1019. <https://doi.org/10.1016/J.MRI.2009.02.004>.
- Biswal, B., F. Z. Yetkin, V. M. Haughton, and J. S. Hyde. 1995. "Functional Connectivity in the Motor Cortex of Resting Human Brain Using Echo-Planar Mri." *Magnetic Resonance in Medicine* 34, no. 4: 537–541. <https://doi.org/10.1002/MRM.1910340409>.
- Biswal, B. B., M. Mennes, X. N. Zuo, et al. 2010. "Toward Discovery Science of Human Brain Function." *Proceedings of the National Academy of Sciences of the United States of America* 107, no. 10: 4734–4739. [https://doi.org/10.1073/PNAS.0911855107/SUPPL\\_FILE/PNAS.200911855SI.PDF](https://doi.org/10.1073/PNAS.0911855107/SUPPL_FILE/PNAS.200911855SI.PDF).
- Bright, M. G., C. R. Tench, and K. Murphy. 2017. "Potential Pitfalls When Denoising Resting State fMRI Data Using Nuisance Regression." *NeuroImage* 154: 159–168. <https://doi.org/10.1016/J.NEUROIMAGE.2016.12.027>.
- Ciric, R., D. H. Wolf, J. D. Power, et al. 2017. "Benchmarking of Participant-Level Confound Regression Strategies for the Control of Motion Artifact in Studies of Functional Connectivity." *NeuroImage* 154: 174–187. <https://doi.org/10.1016/J.NEUROIMAGE.2017.03.020>.
- Craddock, R. C., P. E. Holtzheimer, X. P. Hu, and H. S. Mayberg. 2012. "A Whole Brain fMRI Atlas Generated via Spatially Constrained Spectral Clustering." *Human Brain Mapping* 33, no. 8: 1914–1928. <https://doi.org/10.1002/HBM.21333>.
- Demertzi, A., A. Kucyi, A. Ponce-Alvarez, G. A. Keliris, S. Whitfield-Gabrieli, and G. Deco. 2022. "Functional Network Antagonism and Consciousness." *Network Neuroscience* 6, no. 4: 998–1009. [https://doi.org/10.1162/netn\\_a\\_00244](https://doi.org/10.1162/netn_a_00244).
- Dubois, J., and R. Adolphs. 2016. "Building a Science of Individual Differences From fMRI." *Trends in Cognitive Sciences* 20, no. 6: 425–443. <https://doi.org/10.1016/j.tics.2016.03.014>.
- Eickhoff, S. B., B. T. T. Yeo, and S. Genon. 2018. "Imaging-Based Parcellations of the Human Brain." *Nature Reviews Neuroscience* 19, no. 11: 672–686. <https://doi.org/10.1038/s41583-018-0071-7>.
- Finn, E. S., and R. T. Constable. 2016. "Individual Variation in Functional Brain Connectivity: Implications for Personalized Approaches to Psychiatric Disease." *Dialogues in Clinical Neuroscience* 18, no. 3: 277–287. <https://doi.org/10.31887/DCNS.2016.18.3/EFINN>.
- Finn, E. S., and M. D. Rosenberg. 2021. "Beyond Fingerprinting: Choosing Predictive Connectomes Over Reliable Connectomes." *NeuroImage* 239: 118254. <https://doi.org/10.1016/J.NEUROIMAGE.2021.118254>.
- Finn, E. S., X. Shen, D. Scheinost, et al. 2015. "Functional Connectome Fingerprinting: Identifying Individuals Using Patterns of Brain Connectivity." *Nature Neuroscience* 18, no. 11: 1664–1671. <https://doi.org/10.1038/nn.4135>.
- Fox, M. D., and M. E. Raichle. 2007. "Spontaneous Fluctuations in Brain Activity Observed With Functional Magnetic Resonance Imaging." *Nature Reviews Neuroscience* 8, no. 9: 700–711. <https://doi.org/10.1038/nrn2201>.
- Fox, M. D., D. Zhang, A. Z. Snyder, and M. E. Raichle. 2009. "The Global Signal and Observed Anticorrelated Resting State Brain Networks." *Journal of Neurophysiology* 101, no. 6: 3270–3283. <https://doi.org/10.1152/jn.90777.2008>.
- Friston, K. J. 2011. "Functional and Effective Connectivity: A Review." *Brain Connectivity* 1, no. 1: 13–36. <https://doi.org/10.1089/brain.2011.0008>.
- Friston, K. J., J. Ashburner, S. Kiebel, T. Nichols, and W. Penny. 2007. *Statistical parametric mapping: The analysis of functional brain images*. Academic Press. <https://doi.org/10.1016/B978-0-12-372560-8.X5000-1>.
- Friston, K. J., P. Rotshtein, J. J. Geng, P. Sterzer, and R. N. Henson. 2006. "A Critique of Functional Localisers." *NeuroImage* 30, no. 4: 1077–1087. <https://doi.org/10.1016/j.neuroimage.2005.08.012>.
- Friston, K. J., S. Williams, R. Howard, R. S. J. Frackowiak, and R. Turner. 1996. "Movement-Related Effects in fMRI Time-Series." *Magnetic Resonance in Medicine* 35, no. 3: 346–355. <https://doi.org/10.1002/MRM.1910350312>.
- Geerligs, L., M. Rubinov, L. K. Tyler, et al. 2015. "State and Trait Components of Functional Connectivity: Individual Differences Vary With Mental State." *Journal of Neuroscience* 35, no. 41: 13949–13961. <https://doi.org/10.1523/JNEUROSCI.1324-15.2015>.
- Glasser, M. F., S. N. Sotiropoulos, J. A. Wilson, et al. 2013. "The Minimal Preprocessing Pipelines for the Human Connectome Project." *NeuroImage* 80: 105–124. <https://doi.org/10.1016/J.NEUROIMAGE.2013.04.127>.
- Gordon, E. M., T. O. Laumann, A. W. Gilmore, et al. 2017. "Precision Functional Mapping of Individual Human Brains." *Neuron* 95, no. 4: 791–807. <https://doi.org/10.1016/J.NEURON.2017.07.011>.
- Grabner, G., A. L. Janke, M. M. Budge, D. Smith, J. Pruessner, and D. L. Collins. 2006. "Symmetric Atlasing and Model Based Segmentation: An Application to the Hippocampus in Older Adults." In *Lecture Notes in Computer Science (Including Subseries Lecture Notes in Artificial Intelligence and Lecture Notes in Bioinformatics)*, 4191 LNCS-II, 58–66. Springer Berlin Heidelberg. [https://doi.org/10.1007/11866763\\_8/COVER](https://doi.org/10.1007/11866763_8/COVER).
- Gratton, C., T. O. Laumann, A. N. Nielsen, et al. 2018. "Functional Brain Networks Are Dominated by Stable Group and Individual Factors, Not Cognitive or Daily Variation." *Neuron* 98, no. 2: 439–452.e5. <https://doi.org/10.1016/j.neuron.2018.03.035>.
- Hamdan, S., S. More, L. Sasse, V. Komeyer, K. R. Patil, and F. Raimondo. 2023. "Julearn: An Easy-to-Use Library for Leakage-Free Evaluation and Inspection of ML Models." <https://doi.org/10.48550/arXiv.2310.12568>.

- Hastie, T., R. Tibshirani, and J. Friedman. 2009. *The Elements of Statistical Learning: Data Mining, Inference, and Prediction*. 2nd ed. Springer.
- He, T., R. Kong, A. J. Holmes, et al. 2020. "Deep Neural Networks and Kernel Regression Achieve Comparable Accuracies for Functional Connectivity Prediction of Behavior and Demographics." *NeuroImage* 206: 116276. <https://doi.org/10.1016/J.NEUROIMAGE.2019.116276>.
- Horien, C., S. Noble, E. S. Finn, X. Shen, D. Scheinost, and R. T. Constable. 2018. "Considering Factors Affecting the Connectome-Based Identification Process: Comment on Waller et al." *NeuroImage* 169: 172–175. <https://doi.org/10.1016/J.NEUROIMAGE.2017.12.045>.
- Horien, C., X. Shen, D. Scheinost, and R. T. Constable. 2019. "The Individual Functional Connectome Is Unique and Stable Over Months to Years." *NeuroImage* 189: 676–687. <https://doi.org/10.1016/j.neuroimage.2019.02.002>.
- Jenkinson, M., C. F. Beckmann, T. E. J. Behrens, M. W. Woolrich, and S. M. Smith. 2012. "FSL." *NeuroImage* 62, no. 2: 782–790. <https://doi.org/10.1016/j.neuroimage.2011.09.015>.
- Kong, R., J. Li, C. Orban, et al. 2019. "Spatial Topography of Individual-Specific Cortical Networks Predicts Human Cognition, Personality, and Emotion." *Cerebral Cortex* 29, no. 6: 2533–2551. <https://doi.org/10.1093/CERCOR/BHY123>.
- Kong, R., Q. Yang, E. Gordon, et al. 2021. "Individual-Specific Areal-Level Parcellations Improve Functional Connectivity Prediction of Behavior." *Cerebral Cortex* 31, no. 10: 4477–4500. <https://doi.org/10.1093/CERCOR/BHAB101>.
- Kopal, J., A. Pidnebesna, D. Tomeček, J. Tintěra, and J. Hlinka. 2020. "Typicality of Functional Connectivity Robustly Captures Motion Artifacts in Rs-fMRI Across Datasets, Atlases, and Preprocessing Pipelines." *Human Brain Mapping* 41, no. 18: 5325–5340. <https://doi.org/10.1002/hbm.25195>.
- Korhonen, O., H. Saarimäki, E. Glerean, M. Sams, J. Saramäki, and X. Zuo. 2017. "Consistency of Regions of Interest as Nodes of fMRI Functional Brain Networks." *Network Neuroscience* 1, no. 3: 254–274. [https://doi.org/10.1162/NETN\\_A\\_00013](https://doi.org/10.1162/NETN_A_00013).
- Leopold, D. A., Y. Murayama, and N. K. Logothetis. 2003. "Very Slow Activity Fluctuations in Monkey Visual Cortex: Implications for Functional Brain Imaging." *Cerebral Cortex* 13, no. 4: 422–433. <https://doi.org/10.1093/cercor/13.4.422>.
- Li, J., R. Kong, R. Liégeois, et al. 2019. "Global Signal Regression Strengthens Association Between Resting-State Functional Connectivity and Behavior." *NeuroImage* 196: 126–141. <https://doi.org/10.1016/J.NEUROIMAGE.2019.04.016>.
- Li, K., K. Wisner, and G. Atluri. 2021. "Feature Selection Framework for Functional Connectome Fingerprinting." *Human Brain Mapping* 42, no. 12: 3717–3732. <https://doi.org/10.1002/hbm.25379>.
- Lindquist, M. A., S. Geuter, T. D. Wager, and B. S. Caffo. 2019. "Modular Preprocessing Pipelines Can Reintroduce Artifacts Into fMRI Data." *Human Brain Mapping* 40, no. 8: 2358–2376. <https://doi.org/10.1002/HBM.24528>.
- Logothetis, N. K. 2003. "The Underpinnings of the BOLD Functional Magnetic Resonance Imaging Signal." *Journal of Neuroscience* 23, no. 10: 3963–3971. <https://doi.org/10.1523/JNEUROSCI.23-10-03963.2003>.
- Macey, P. M., K. E. Macey, R. Kumar, and R. M. Harper. 2004. "A Method for Removal of Global Effects From fMRI Time Series." *NeuroImage* 22, no. 1: 360–366. <https://doi.org/10.1016/j.neuroimage.2003.12.042>.
- Mantwill, M., M. Gell, S. Krohn, and C. Finke. 2022. "Brain Connectivity Fingerprinting and Behavioural Prediction Rest on Distinct Functional Systems of the Human Connectome." *Communications Biology* 5, no. 1: 1–10. <https://doi.org/10.1038/s42003-022-03185-3>.
- More, S., G. Antonopoulos, F. Hoffstaedter, J. Caspers, S. B. Eickhoff, and K. R. Patil. 2023. "Brain-Age Prediction: A Systematic Comparison of Machine Learning Workflows." *NeuroImage* 270: 119947. <https://doi.org/10.1016/j.neuroimage.2023.119947>.
- Nadeau, C., and Y. Bengio. 2003. "Inference for the Generalization Error." *Machine Learning* 52, no. 3: 239–281. <https://doi.org/10.1023/A:1024068626366>.
- Noble, S., D. Scheinost, and R. T. Constable. 2019. "A Decade of Test-Retest Reliability of Functional Connectivity: A Systematic Review and Meta-Analysis." *NeuroImage* 203: 116157. <https://doi.org/10.1016/J.NEUROIMAGE.2019.116157>.
- Parkes, L., B. Fulcher, M. Yücel, and A. Fornito. 2018. "An Evaluation of the Efficacy, Reliability, and Sensitivity of Motion Correction Strategies for Resting-State Functional MRI." *NeuroImage* 171: 415–436. <https://doi.org/10.1016/j.neuroimage.2017.12.073>.
- Pedregosa, F., G. Varoquaux, A. Gramfort, et al. 2011. "Scikit-Learn: Machine Learning in Python." *Journal of Machine Learning Research* 12: 2825–2830.
- Pernet, C. R., R. Wilcox, and G. A. Rousselet. 2013. "Robust Correlation Analyses: False Positive and Power Validation Using a New Open Source Matlab Toolbox." *Frontiers in Psychology* 3: 606. <https://doi.org/10.3389/FPSYG.2012.00606/BIBTEX>.
- Power, J. D., M. Plitt, T. O. Laumann, and A. Martin. 2017. "Sources and Implications of Whole-Brain fMRI Signals in Humans." *NeuroImage* 146: 609–625. <https://doi.org/10.1016/j.neuroimage.2016.09.038>.
- Power, J. D., B. L. Schlaggar, and S. E. Petersen. 2014. "Studying Brain Organization via Spontaneous fMRI Signal." *Neuron* 84, no. 4: 681–696. <https://doi.org/10.1016/J.NEURON.2014.09.007>.
- Power, J. D., B. L. Schlaggar, and S. E. Petersen. 2015. "Recent Progress and Outstanding Issues in Motion Correction in Resting State fMRI." *NeuroImage* 105: 536–551. <https://doi.org/10.1016/J.NEUROIMAGE.2014.10.044>.
- Salimi-Khorshidi, G., G. Douaud, C. F. Beckmann, M. F. Glasser, L. Griffanti, and S. M. Smith. 2014. "Automatic Denoising of Functional MRI Data: Combining Independent Component Analysis and Hierarchical Fusion of Classifiers." *NeuroImage* 90: 449–468. <https://doi.org/10.1016/j.neuroimage.2013.11.046>.
- Sasse, L., D. I. Larabi, A. Omidvarnia, et al. 2023. "Intermediately Synchronised Brain States Optimise Trade-Off Between Subject Specificity and Predictive Capacity." *Communications Biology* 6, no. 1: 1–14. <https://doi.org/10.1038/s42003-023-05073-w>.
- Satterthwaite, T. D., M. A. Elliott, R. T. Gerraty, et al. 2013. "An Improved Framework for Confound Regression and Filtering for Control of Motion Artifact in the Preprocessing of Resting-State Functional Connectivity Data." *NeuroImage* 64: 240–256. <https://doi.org/10.1016/j.neuroimage.2012.08.052>.
- Saxe, R., M. Brett, and N. Kanwisher. 2006. "Divide and Conquer: A Defense of Functional Localizers." *NeuroImage* 30, no. 4: 1088–1096. <https://doi.org/10.1016/j.neuroimage.2005.12.062>.
- Schaefer, A., R. Kong, E. M. Gordon, et al. 2018. "Local-Global Parcellation of the Human Cerebral Cortex From Intrinsic Functional Connectivity MRI." *Cerebral Cortex* 28, no. 9: 3095–3114. <https://doi.org/10.1093/CERCOR/BHX179>.
- Schulz, M.-A., D. Bzdok, S. Haufe, J.-D. Haynes, and K. Ritter. 2024. "Performance Reserves in Brain-Imaging-Based Phenotype Prediction." *Cell Reports* 43, no. 1: 113597. <https://doi.org/10.1016/j.celrep.2023.113597>.
- Shen, X., F. Tokoglu, X. Papademetris, and R. T. Constable. 2013. "Groupwise Whole-Brain Parcellation From Resting-State fMRI Data for Network Node Identification." *NeuroImage* 82: 403–415. <https://doi.org/10.1016/j.neuroimage.2013.05.081>.
- Siegel, J. S., A. Mitra, T. O. Laumann, et al. 2017. "Data Quality Influences Observed Links Between Functional Connectivity and Behavior." *Cerebral Cortex* 27, no. 9: 4492–4502. <https://doi.org/10.1093/CERCOR/BHW253>.

Smith, S. M., C. F. Beckmann, J. Andersson, et al. 2013. "Resting-State fMRI in the Human Connectome Project." *NeuroImage* 80: 144–168. <https://doi.org/10.1016/j.NEUROIMAGE.2013.05.039>.

Snoek, L., S. Miletić, and H. S. Scholte. 2019. "How to Control for Confounds in Decoding Analyses of Neuroimaging Data." *NeuroImage* 184: 741–760. <https://doi.org/10.1016/j.NEUROIMAGE.2018.09.074>.

Stanley, M. L., M. N. Moussa, B. M. Paolini, R. G. Lyday, J. H. Burdette, and P. J. Laurienti. 2013. "Defining Nodes in Complex Brain Networks." *Frontiers in Computational Neuroscience* 7: 169. <https://doi.org/10.3389/fncom.2013.00169>.

Thiele, J. A., J. Faskowitz, O. Sporns, and K. Hilger. 2024. "Choosing Explanation Over Performance: Insights From Machine Learning-Based Prediction of Human Intelligence From Brain Connectivity." *PNAS Nexus* 3, no. 12: pgae519. <https://doi.org/10.1093/pnasnexus/pgae519>.

Uğurbil, K., J. Xu, E. J. Auerbach, et al. 2013. "Pushing Spatial and Temporal Resolution for Functional and Diffusion MRI in the Human Connectome Project." *NeuroImage* 80: 80–104. <https://doi.org/10.1016/j.neuroimage.2013.05.012>.

Van Essen, D. C., S. M. Smith, D. M. Barch, T. E. J. Behrens, E. Yacoub, and K. Ugurbil. 2013. "The WU-Minn Human Connectome Project: An Overview." *NeuroImage* 80: 62–79. <https://doi.org/10.1016/j.neuroimage.2013.05.041>.

Waller, L., H. Walter, J. D. Kruschwitz, et al. 2017. "Evaluating the Replicability, Specificity, and Generalizability of Connectome Fingerprints." *NeuroImage* 158: 371–377. <https://doi.org/10.1016/j.NEUROIMAGE.2017.07.016>.

Whitfield-Gabrieli, S., and A. Nieto-Castanon. 2012. "Conn: A functional connectivity toolbox for correlated and anticorrelated brain networks." *Brain Connectivity* 2, no. 3: 125–141. <https://doi.org/10.1089/brain.2012.0073>.

Yamada, T., R.-I. Hashimoto, N. Yahata, et al. 2017. "Resting-State Functional Connectivity-Based Biomarkers and Functional MRI-Based Neurofeedback for Psychiatric Disorders: A Challenge for Developing Theranostic Biomarkers." *International Journal of Neuropsychopharmacology* 20, no. 10: 769–781. <https://doi.org/10.1093/ijnp/pyx059>.

Yan, C. G., B. Cheung, C. Kelly, et al. 2013. "A Comprehensive Assessment of Regional Variation in the Impact of Head Micromovements on Functional Connectomics." *NeuroImage* 76: 183–201. <https://doi.org/10.1016/j.NEUROIMAGE.2013.03.004>.

Yoshimoto, T., K. Tokunaga, and J. Chikazoe. 2024. "Enhancing Prediction of Human Traits and Behaviors Through Ensemble Learning of Traditional and Novel Resting-State fMRI Connectivity Analyses." *NeuroImage* 303: 120911. <https://doi.org/10.1016/j.neuroimage.2024.120911>.

## Supporting Information

Additional supporting information can be found online in the Supporting Information section. **Figure S1:** Comparing identification performance of rs-FC denoised at the voxel- versus region-level across Mean or EV aggregation (shape) and three parcellation granularities in both data quality configurations (color). (a) Identification accuracy increases with finer granularities. Differences between the denoising levels are observed only in the case of EV aggregation. (b) Differential Identifiability also increases with finer parcellation. Deviations from the diagonal only occur in EV aggregation in favor of voxel-level denoising at 100 regions and equal or better for region-level denoising at 400 and 1000 regions. **Figure S2:** Overview of individual specificity of rs-FC across parcellation granularities. Results are shown for rs-FC generated from *Minimal* (a, c) and *ICA-FIX* (b, d) data configuration. **Figure S3:** Within- and between-subject correlations (Fisher z-transformed) from Rest1 to Rest2. (a, b) Within-subject correlations in both data configurations per subject ( $n = 370$ ). (c, d) Average between-subject correlations in both data configurations per subject ( $n = 370$ ). Statistical analyses

were conducted separately per data configuration. Post hoc Bonferroni corrected pairwise  $t$ -tests across all groups were significant ( $p < 0.05$ ), unless indicated otherwise (ns). **Figure S12:** Typicality of FC values per condition. Showing Fisher z-transformed correlation between each individual's FC ( $n = 370$ ) and the group average FC for each condition. Statistical comparisons between all groups within each data configuration were significant ( $p < 0.05$ ) unless indicated otherwise. TFC values did not differ between voxel-wise and region-wise denoising for mean aggregation within the same parcellation granularity. In the 100 region parcellation no differences were found comparing both Mean aggregated approaches with the region-wise denoised TFC values when EV aggregation was used. **Table S4:** Summary statistics for within-subject correlations (Fisher z-transformed) from Rest1 to Rest2. **Table S5:** ANOVA table for within-subject correlations (Fisher z-transformed) from Rest1 to Rest2. Analyses were performed separately per data configuration.  $p$  values smaller than 0.0000 are set to 0. **Table S6:** Post hoc group-wise comparisons for within-subject correlations (Fisher z-transformed) from Rest1 to Rest2. Analyses were performed separately per data configuration. Two-sided pairwise  $t$ -tests were computed.  $p$  values were Bonferroni corrected for multiple comparisons. Group labels are constructed as (denoising level\_parcellation granularity (regions)\_aggregation method).  $p$  values smaller than 0.0000 are set to 0. **Table S7:** Summary statistics for between-subject correlations (Fisher z-transformed) from Rest1 to Rest2. **Table S8:** ANOVA table for between-subject correlations (Fisher z-transformed) from Rest1 to Rest2. Analyses were performed separately per data configuration.  $p$  values smaller than 0.0000 are set to 0. **Table S9:** Post hoc group-wise comparisons for barison of time required to preprocess and calculate between-subject correlations (Fisher z-transformed) from Rest1 to Rest2. Analyses were performed separately per data configuration. Two-sided pairwise  $t$ -tests were computed.  $p$  values were Bonferroni corrected for multiple comparisons. Group labels are constructed as (denoising level\_parcellation granularity (regions)\_aggregation method).  $p$  values smaller than 0.0000 are set to 0. **Table S10:** Overview of significant post hoc model score comparisons. Paired  $t$ -tests were performed within each data configuration on all model scores per target.  $p$  values were corrected using Bonferroni correction. Group names are constructed as (parcellation granularity (regions)\_Denoising level\_aggregation method). **Table S11:** Overview of TFC similarity with mean FD per single scan. Similarity is computed as Spearman's correlation of TFC values versus mean framewise displacement values (subject-wise). Reported are the correlation coefficients and associated  $p$  values.  $p$  values smaller than 0.0000 are set to 0. **Table S13:** Summary statistics for TFC correlations (Fisher z-transformed) from individual FC to group FC. Averaged across sessions and phase-encoding per subject. **Table S14:** ANOVA table for TFC correlations (Fisher z-transformed) from individual FC to group FC. Analyses were performed separately per data configuration. Averaged across sessions and phase-encoding per subject.  $p$  values smaller than 0.0000 are set to 0. **Table S15:** Post hoc group-wise comparisons for TFC correlations (Fisher z-transformed) from individual FC to group FC. Analyses were performed separately per data configuration. Averaged across sessions and phase-encoding per subject. Two-sided pairwise  $t$ -tests were computed.  $p$  values were Bonferroni corrected for multiple comparisons. Group labels are constructed as (denoising level \_ parcellation granularity (regions)\_aggregation method).  $p$  values smaller than 0.0000 are set to 0. **Table S16:** Summary statistics for pipeline runtime in seconds. Averaged across sessions, phase-encoding, and data configuration. **Table S17:** ANOVA table for pipeline runtime. Averaged across sessions, phase-encoding, and data configuration.  $p$  values smaller than 0.0000 are set to 0. **Table S18:** Post hoc group-wise comparisons for pipeline runtime. Averaged across sessions, phase-encoding, and data configuration. Two-sided pairwise  $t$ -tests were computed.  $p$  values were Bonferroni corrected for multiple comparisons. Group labels are constructed as (denoising level\_parcellation granularity (regions)\_aggregation method).  $p$  values smaller than 0.0000 are set to 0. **Table S19:** Group-level variance explained by the first eigenvariate across the whole brain per scan. Averaged across all regions and subjects. Cases of computational inaccuracy were handled by rounding to the nearest possible value (max: 1.0, min: 0.0).